Ecological Indicators 159 (2024) 111689

Contents lists available at ScienceDirect

Ecological Indicators

journal homepage: www.elsevier.com/locate/ecolind

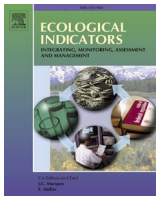

Original Articles

Holistic evolution of ecosystem in Heihe River Basin from the perspective of eigen microstates

Xu Wang [a], Hao Fan [b,*], Xiaosong Chen [a,*], Yiran Xie [c], Hongyu Wang [a]

[a] School of Systems Science/Institute of Nonequilibrium Systems, Beijing Normal University, Beijing 100875, China
[b] School of Environment, Beijing Normal University, Beijing, 100875, China
[c] School of National Safety and Emergency Management, Beijing Normal University, Zhuhai, 519087, China

ARTICLE INFO

Keywords:
NDVI
Soil moisture
Eigen microstates
Heihe River Basin

ABSTRACT

The impact of environmental change on vegetation dynamics plays a key role in ecosystem evolution, with vegetation demonstrating heightened sensitivity to both climate fluctuations and human activities. However, existing studies have not fully unveiled the emergence of vegetation evolution patterns within the holistic complex systems framework. Based on long-term observational data of the normalized differential vegetation index (NDVI) and meteorological reanalysis data, this study used the mean synthesis and trend analysis methods to explore the spatial distribution and temporal variation of NDVI in the Heihe River Basin (HRB). The results show that a continuous NDVI increase in the HRB from 1982 to 2015, and the growth rate post-2000 being 1.66 times higher than pre-2000, with distinct seasonal periodic fluctuations. Spatially, vegetation thrives predominantly in the upstream and downstream riparian zones of the HRB, displaying significant spatial heterogeneity, and it shows an obvious increasing trend in the middle and lower reaches, especially after 2000. We built a theoretical method using eigen microstates to quantify the dynamic changes in ecosystem vegetation. The first two microstates can account for 64% of the NDVI variations, among which the first microstate captures the overall uptrend and seasonal periodicity of NDVI, while the second microstate highlights the key contributions of soil moisture to vegetation growth. In HRB, soil moisture emerges as the most influential factor for vegetation improvement, surpassing other meteorological variables. Meanwhile, there's a one-month lag in vegetation response to soil moisture, and deeper soil moisture exerts a more pronounced effect on vegetation coverage. This study not only validates the effective applicability of eigen microstates for identifying and attributing ecosystem changes but also provides a new perspective for comprehending the impact of soil moisture on vegetation dynamics.

1. Introduction

Vegetation comprises a pivotal constituent within terrestrial ecosystems, serving as the fundamental substrate for the entire ecological framework. Extensive research has highlighted its central role in the complex global carbon cycle dynamics (Ciais et al., 2005; Jiang et al., 2022; Peylin et al., 2005). Simultaneously, it functions as a discerning barometer of ecosystem vitality, proficiently manifesting perturbations induced by external environmental fluxes (Peng et al., 2011; Piao et al., 2011; Zhao et al., 2018). Over recent decades, terrestrial ecosystems have undergone notable regional transformations, attributed to the conjoined influences of anthropogenic activities and climatic shifts, as substantiated in prior studies (Jiang et al., 2017; Kariyeva and Van Leeuwen, 2011; Peñuelas et al., 2002). Consequently, long-term systematic alterations in vegetative cover have become a forefront and focal area of research in contemporary ecological discourse (Chu et al., 2019; Park and Sohn, 2010).

The second largest inland river basin in China, the Heihe River, originates in the Tibetan Plateau and extends northward to arid and semi-arid territories, encompassing three distinct ecosystems-mountains, oases, and deserts-which collectively form a prototypical complex ecosystem. In recent years, scholarly attention has increasingly focused on subjects related to vegetation dynamics, water resource allocation, and climate fluctuations within the HRB (Ma and Frank, 2006; Geng et al., 2014; You et al., 2018). Researchers utilized NDVI to analyze vegetation change patterns and their correlation with

* Corresponding authors.
E-mail addresses: fanhao_geo@163.com (H. Fan), chenxs@bnu.edu.cn (X. Chen).

https://doi.org/10.1016/j.ecolind.2024.111689
Received 14 November 2023; Received in revised form 14 January 2024; Accepted 31 January 2024
Available online 9 February 2024

meteorological variables in the upper, middle, and lower segments of the HRB from 1982 to 2015, with a specific focus on the period post-2000 (Yuan et al., 2019a). Scholars particularly highlighted the diverse impacts of ecological engineering endeavors on different geographical regions and vegetation categories within the basin (Chang et al., 2011). Using EVI, researchers observed noticeable variations in vegetation change patterns among these segments, displaying an overall increasing trend across years. The upper regions predominantly exhibited responsiveness to temperature and precipitation, while surface runoff emerged as the principal influencer in the middle and lower regions (Xiao et al., 2015; You et al., 2018). Furthermore, someone devised a GPP estimation technique, providing deeper insights into the distinct influences of climate-driven factors across diverse river basins within the HRB (You et al., 2020). But there remains a lack of understanding regarding shifts in ecosystem stability and the fundamental drivers impacting the vegetation ecosystem in the HRB. Therefore, it is imperative to investigate the enduring transformations of regional ecosystems, with a specific emphasis on vegetation, through the adoption of a holistic and intricate systems perspective.

Scholars worldwide have long conducted extensive research on vegetation changes and ecosystems, underscoring the central role of ecosystem stability in ecology (Ives and Carpenter, 2007). The establishment of prolonged vegetation monitoring serves as a foundational underpinning for uncovering the determinants of change and delving into the dynamics of ecosystems (De Jong et al., 2013; Verbesselt et al., 2010; Virtanen et al., 2010). Previous research often adopted a reductionist framework, involving the direct correlation of regional and categorical vegetation indices with meteorological variables such as precipitation, radiation, and temperature (Lamchin et al., 2018; Liu and Lei, 2015; Xu et al., 2014; Xu et al., 2017). It allows for a relatively expedited evaluation assessment of the impact of meteorological factors on vegetation changes within specific geographical regions, types, and temporal intervals. Nevertheless, it falls short in its ability to discern the presence of systematic changes within regional ecosystems or in elucidating inherent global characteristics.

Statistical physics-based research methodologies have proven to be instrumental in analyzing complex Earth systems, yielding valuable insights into our understanding of the climate system. For example, by employing the critical point identification and prediction method, researchers have discovered a robust negative teleconnection between the Amazon Rainforest Area and the TP, and it has led to the indication that the TP should be considered as a candidate for inclusion in the list of tipping elements (Lenton et al., 2019; Liu et al., 2023). Furthermore, the eigen microstates method, which is based on the theoretical framework of statistical physics, has been successfully applied to the study of non-equilibrium complex systems with unknown order parameters. For instance, in the context of Earth system climate patterns, the analysis of the six primary eigen microstates and their evolutions has unveiled insights into the seasonal cycle, land-sea temperature contrast, tropical warming, semiannual oscillations, and El Niño (Sun et al., 2021). Additionally, when examining the ozone mass mixing ratio (OMMR) at varying geopotential heights, the first eigen microstate has illuminated changes in atmospheric structure, the overall trend of OMMR, and has facilitated the identification of phenomena such as the El Niño Southern Oscillation (ENSO) and the Quasi-Biennial Oscillation (Chen et al., 2021). In addition, this method has also demonstrated that the strengths of the two major eigen microstates of temperature in the tropics vary significantly with the interannual variability of ENSO (Zhang et al., 2020).

Undoubtedly, the eigen microstate method has furnished a comprehensive and efficacious explanation of emerging phenomena and evolutionary mechanisms within non-equilibrium complex systems. Consequently, we are incorporating this method to explore the global variations in NDVI across the HRB. Our objective is to validate the method's suitability in studying this complex ecological system in HRB, quantifying systematic alterations in both vegetation and meteorological components within this locale, and uncovering the key factors of vegetation changes from diverse microstate perspectives. This approach may provide a more profound avenue for attaining a comprehensive grasp of the perennial ecological evolution patterns.

2. Data and methods

2.1. Study area

The HRB (37°N-43°N, 97°E-102°E, Fig. 1) situated within the arid and semi-arid regions of northwestern China, stands as the second-largest inland river in this geographical expanse, spanning a primary course of 821 km. The basin comprises a rich tapestry of ecological environments, including glaciers, alpine meadows, forests, irrigated farmlands and deserts (Cheng et al., 2014). The headwaters, nestled in the Qilian Mountains, draw upon glacier meltwater contributions and display robust vegetation coverage. The middle Hexi Corridor is characterized by meager precipitation, substantial evaporation and significant irrigation. The downstream area mainly consists of deserts and barren landscapes, marking a region where the river's flow diminishes (Cheng et al., 2014; Fan et al., 2018). The solitary Ejina Oasis in the downstream area serves as both a critical natural buffer for ecological preservation and a vital habitat for the local population's sustenance (Jiang and Liu, 2010; Zang and Liu, 2013).

The HRB is ecologically vulnerable, characterized by annual precipitation levels below 500 mm, sparse vegetation and severe desertification (Nian et al., 2014; Chen et al., 2014). Since the 20th century, rapid population growth and economic development have resulted in changes in land use as well as ecological patterns, leading to a critical ecological predicament (Fan et al., 2018). Therefore, this study aims to quantitatively depict the holistic and general rules, commencing with an analysis of the vegetation ecological processes in the HRB.

2.2. Data

The NDVI data used in this work is sourced from the Global Inventory Monitoring and Modelling System (GIMMS) NDVI3g v1.0 dataset covering the period from 1982 to 2015 (https://ecocast.arc.nasa.gov/data/pub/gimms/). And it has a temporal resolution of 15 days and a spatial resolution of 1/12° × 1/12°, resulting in 4,320 grids over the entire region. We employ a mean synthesis method, which involves averaging data from two adjacent 15-day time points, to derive monthly average data.

We utilized the ERA5 reanalysis data set of the fifth-generation European Center for Medium-Range Weather Forecasts (ECMWF, https://cds.climate.copernicus.eu/), covering variables the 2 m temperature and precipitation. The ERA5 reanalysis data incorporates expanded data sources, an updated weather prediction model, assimilation system, and enjoys extensive utilization (Rohrer et al., 2020; Guo et al., 2021; Fan et al., 2021; Fan et al., 2023). The spatial resolution is 0.25° × 0.25°. Soil moisture and surface runoff data are procured from ERA5-Land, which has a spatial resolution of 0.1° × 0.1° and comprises four layers, 0–7 cm, 7–28 cm, 29–100 cm and 100–289 cm. ERA5-land provides advantageous reanalysis data with significant spatial and temporal continuity, as well as high spatial and temporal resolution. and it is widely used in the field of environmental geomorphology (Li et al., 2020; Wu et al., 2020).

2.3. Method

2.3.1. Trend analysis

The trend analysis method allows for a more comprehensive portrayal of the temporal dynamics within a specific area (Jiang et al., 2015; Yuan et al., 2019b; Ma and Frank, 2006). In this study, we conducted a regional-scale linear regression analysis to examine the association between NDVI and time, concurrently calculating 95 %

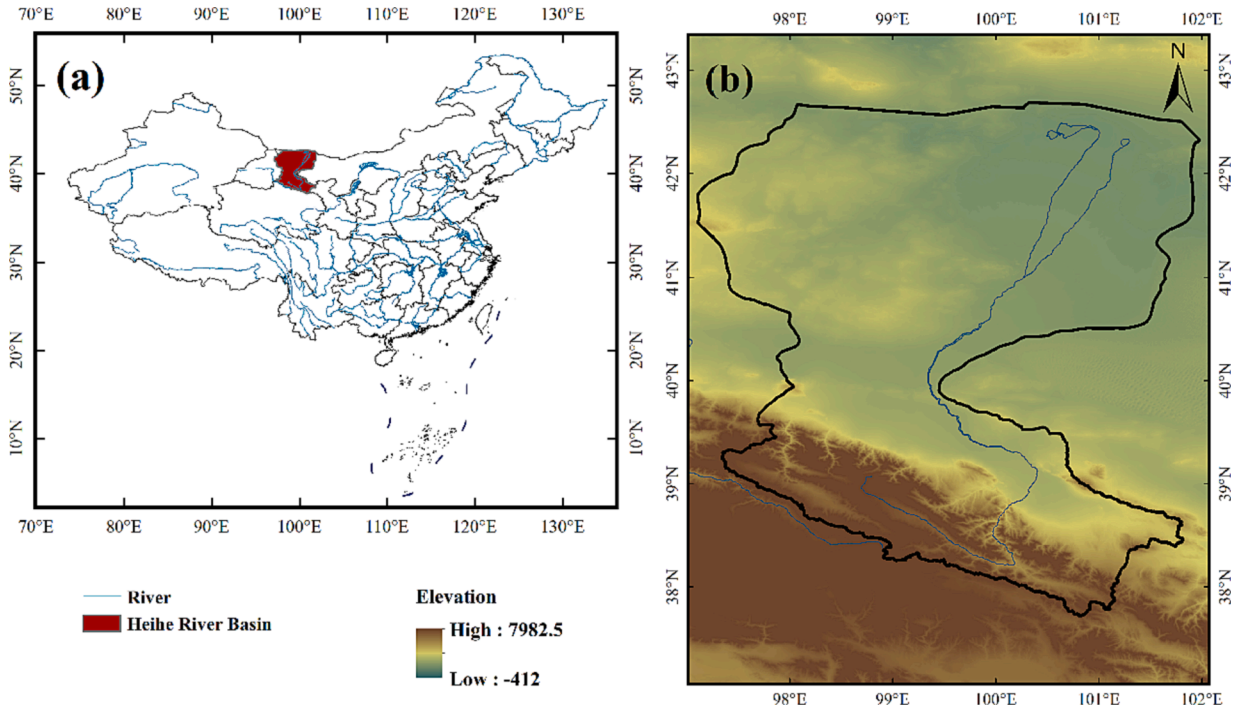

Fig. 1. Elevation and location of the Heihe River Basin, Northwest China.

confidence intervals and verifying the significance of the trend through *t*-test statistics ($P < 0.05$). Simultaneously, it was used to estimate the slope of NDVI on a pixel-wise basis to obtain the spatial multi-year trend, facilitating both monthly and seasonal trend analyses. The slope can be fitted by the observation series $(t, NDVI_i)$ of each grid point:

$$Slope = \frac{\sum_{j=1}^{T}(t_j - \bar{t})(NDVI_j - \overline{NDVI})}{\sum_{j=1}^{T}(t_j - \bar{t})^2} \quad (1)$$

where *Slope* is the trend; $NDVI_j$ is the value at time t_j; when $Slope > 0$, it indicates an upward trend in NDVI over time; when $Slope < 0$, it indicates an downward trend in NDVI over time; T is the cumulative number of months during the study period.

2.3.2. Correlation analysis

Correlation analysis can reveal the interrelationship between the two variables. Pearson's correlation coefficient is commonly used in environmental science and ecology to assess the relationship between climate change and ecosystem dynamics (John et al., 2016; Ichii et al., 2002). Therefore, we chose it for correlation analysis, which was calculated as follows:

$$r = \frac{\sum_{i=1}^{T}(V_{NDVI} - \overline{V}_{NDVI})(V_Y - \overline{V}_Y)}{\sqrt{\sum_{i=1}^{T}(V_{NDVI} - \overline{V}_{NDVI})^2 \sum_{i=1}^{T}(V_Y - \overline{V}_Y)^2}} \quad (2)$$

r falls within the range of [-1,1], signifying both the direction and strength of the trend between the two vectors. Y represents the other variables in the study except NDVI.

2.3.3. Eigen microstate method

The eigen microstate method has good interpretability in analyzing the collective behaviors of complex systems (Sun et al., 2021). We first construct microstates of an ecosystem from NDVI data. For the complex ecosystem composed of N agents, the NDVI at a grid i and time t is $s_i(t)$. The average NDVI at i during the time period T can be calculated as $\overline{s_i} = \frac{1}{T}\sum_{t=1}^{T} s_i(t)$ and the fluctuations of NDVI at the grid i are $\delta s_i(t) = s_i(t) - \overline{s_i(t)}$. Considering the obvious difference in geographical features within the upper and lower reaches of the HRB, substantial disparities in vegetation cover are observed, resulting in significant variations in variance. Thus, we construct the microstate $\delta S(t) = [\delta S_1(t), \delta S_2(t), ..., \delta S_N(t)]^{\mathrm{T}}$ at time t and characterize the fluctuations of NDVI, $S_i(t) = \frac{\delta s_i(t)}{\sqrt{\langle [\delta s_i(t)]^2 \rangle}}$.

Therefore, based on the microstates defined $\delta S(t)$, we can get an $N \times T$ ensemble matrix $\boldsymbol{A}$ with A_{it}:

$$A_{it} = \frac{S_i(t)}{\sqrt{C_0}} \quad (3)$$

where $C_0 = \sum_{t=1}^{T}\sum_{i=1}^{N} S_i^2(t)$.

Considering the correlation of NDVI microstates at t_i, t_j, $C(t_i, t_j) = \delta S(t_i)^{\mathrm{T}} \cdot \delta S(t_j)$, then we can get a $T \times T$ correlation matrix of microstate $\boldsymbol{C} = C_0 \boldsymbol{A}^{\mathrm{T}} \cdot \boldsymbol{A}$ with $C(t_i, t_j)$ as its elements. The matrix $\boldsymbol{C}$ has T eigenvectors $\boldsymbol{v}_j$ of $j = 1, 2, ..., T$ and they can compose a $T \times T$ unitary matrix $\boldsymbol{V} = [\boldsymbol{v}_1, \boldsymbol{v}_2, ..., \boldsymbol{v}_T]$.

The correlation $K_{ij}(T)$ between different grids can be defined as $Kij(T) = \delta S_i \delta S_j^{\mathrm{T}}$, and we can get an $N \times N$ correlation matrix $\boldsymbol{K} = C_0 \boldsymbol{A} \cdot \boldsymbol{A}^{\mathrm{T}}$. The matrix $\boldsymbol{K}$ has N eigenvalues λ_n and N eigenvectors. Then we can obtain $N \times N$ unitary matrix $\boldsymbol{U} = [\boldsymbol{u}_1, \boldsymbol{u}_2, ..., \boldsymbol{u}_N]$.

By using the singular value decomposition (SVD), it is possible to factorize the ensemble matrix $\boldsymbol{A}$ as $\boldsymbol{A} = \boldsymbol{U} \cdot \Lambda \cdot \boldsymbol{V}^{\mathrm{T}} = \sum_{r=1} \sigma_j \boldsymbol{u}_j(T) \otimes (\boldsymbol{v}_j)^{\mathrm{T}}$. The matrix Λ contains the singular values σ_j with its numbering following a sequential order $\sigma_1 \geqslant \sigma_2 \geqslant ... \geqslant \sigma_r$, $r = \min(T, N)$. With $\boldsymbol{K} = C_0 \boldsymbol{A} \cdot \boldsymbol{A}^{\mathrm{T}}$, we can get $\boldsymbol{K} \cdot \boldsymbol{u}_j = C_0 (\sigma_j)^2 \boldsymbol{u}_j$. From $\mathrm{Tr}\mathbf{C} = \mathrm{Tr}\mathbf{K} = C_0$, $\frac{K}{C_0} = 1$,we have the relation $\sum_{i=1}^{T} (\sigma_i)^2 = 1$. The $\boldsymbol{u}_j$ represents the j th eigen microstate and $(\sigma_j)^2$ is the weight. The evolution of the j th eigen microstate can be calculated as $S_j^e = \sum_{i=1}^{N} S_i \boldsymbol{u}_{ij} = \sigma_j \boldsymbol{v}_j$.

Then, we get v_j for the evolution of the j th eigen microstate. And in contrast to the regression method, this approach more accurately captures the overarching dynamic physical mechanisms.

3 Result.

3.1. Analysis of Spatial-Temporal characteristics of NDVI in Heihe River Basin

Fig. 2 shows the spatiotemporal distribution characteristics of NDVI in the HRB. In terms of time (Fig. 2a), with the year 2000 as the dividing line, there is a significant upward trend in NDVI from 1982 to 2000 ($y = 0.0003x + 0.110$, $R^2 = 0.51$, $P < 0.001$), while the growth rate after 2000 is approximately 1.66 times as large as that before 2000, demonstrating a notably increased growth rate ($y = 0.0005x + 0.112$, $R^2 = 0.50$, $P < 0.01$). The monthly mean results in Fig. 2a show consistent seasonal variations before and after 2000. NDVI exhibits a progressive increase from May to August each year, peaking in August. It is worth noting that NDVI after 2000 is higher than that before 2000 mainly in summer and autumn, indicating that vegetation coverage increased faster during this period.

In terms of space, the annual average NDVI in the study area ranges from 0 to 0.5. Approximately 85 % of the regions exhibits a mean value below 0.2, while around 14 % shows values ranging from 0.2 to 0.4, and merely 0.5 % register values exceeding 0.4. This fully portrays the sparse vegetation and low vegetation coverage in HRB. NDVI value in the upper reaches of the HRB is higher compared to the middle and lower reaches. In the lower reaches, the value reaches 0.2, notably in the desert riparian zone of HRB and Ejina Oasis (Fig. 2b). Accordingly, the spatial distribution of NDVI standard deviation corresponds well with its mean value, indicating that the zones with larger standard deviation generally exhibit a greater NDVI mean value (Fig. 2b). Specifically, the study area is mainly residing in arid and semi-arid regions in the middle latitudes of the northern hemisphere, exhibiting distinct seasonal variations in vegetation. Especially, the NDVI values during the growing season and withering period display significant disparities (Zhu et al., 2019). However, the overall NDVI standard deviation in the study area remains small, with a mean value of only 0.04 and a maximum value of approximately 0.23. This suggests that the extent of vegetation fluctuations across the entire area is limited.

We conducted a detailed analysis of the spatiotemporal change trends of vegetation in the two different time periods (Fig. 3). Before 2000, 81 % of the area shows an upward trend in NDVI (in 11.82 % of the area, NDVI increased significantly), and after 2000, 84 % of the area shows an upward trend in NDVI (in 51.36 % of the area, NDVI increased significantly). Thus, the proportion of vegetation with significant increase after 2000 is much larger than that before 2000 (Fig. 3cd). According to the spatial trend chart (Fig. 3ab), the vegetation improvement after 2000 is predominantly concentrated in the middle and lower reaches of the HRB. The existing studies have also identified an increasing trend in NDVI in the HRB, and have attributed these changes to human-induced vegetation enhancements (Ding et al., 2017) as well as the variations of temperature and precipitation (You et al., 2020; Yuan et al., 2019a).

According to the above findings, NDVI in the study area displays distinct seasonal variations (Fig. 2a). We proceeded to conduct a detailed analysis of the spatial distribution patterns and seasonal trends. In terms of space (Fig. 4), the mean values of NDVI for spring, summer, autumn and winter are 0.10, 0.16, 0.11 and 0.09, respectively, and the corresponding maximum values are observed in spring (0.37), summer (0.74), autumn (0.45) and winter (0.34). The highest values of NDVI appear in the forest ecosystem of Qilian Mountains in the upper reaches of the HRB, with NDVI values exceeding 0.7. Particularly NDVI values

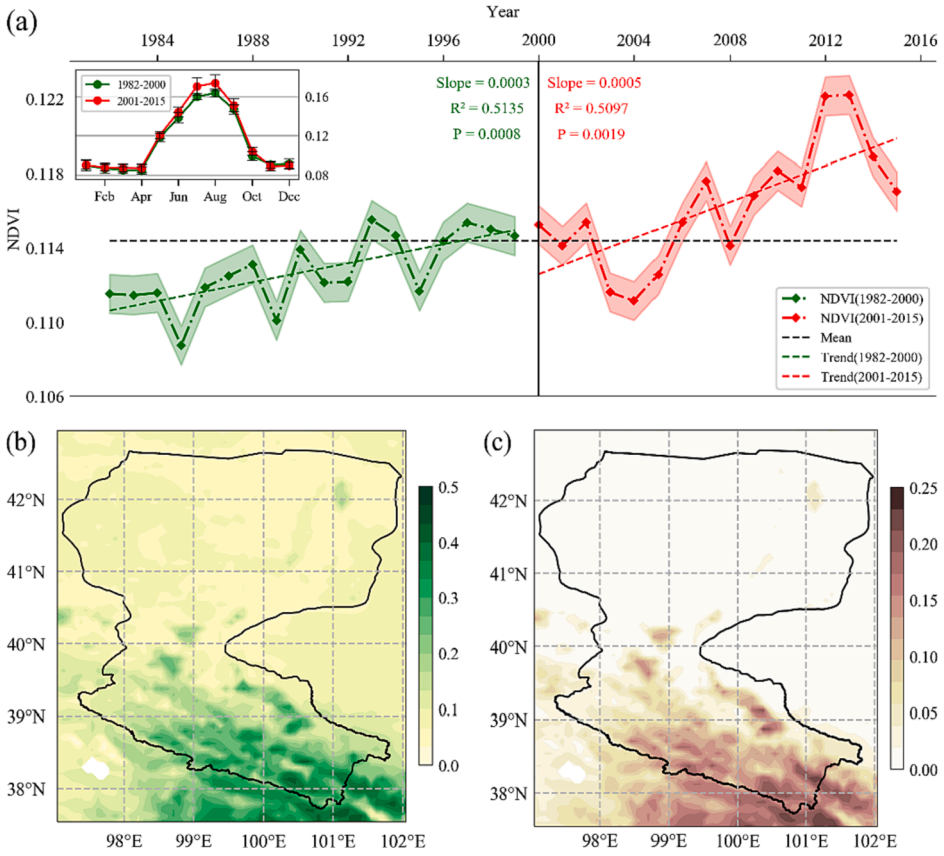

Fig. 2. Time series and spatial distribution of NDVI mean and its standard deviation in Heihe River Basin. (a) Time series of annual NDVI with mean monthly NDVI inset. Shaded area indicate 95 % confidence interval and show the error bars indicate ± 1 SD. (b) The mean value of NDVI from 1982 to 2015. (c) The standard deviation of NDVI from 1982 to 2015.

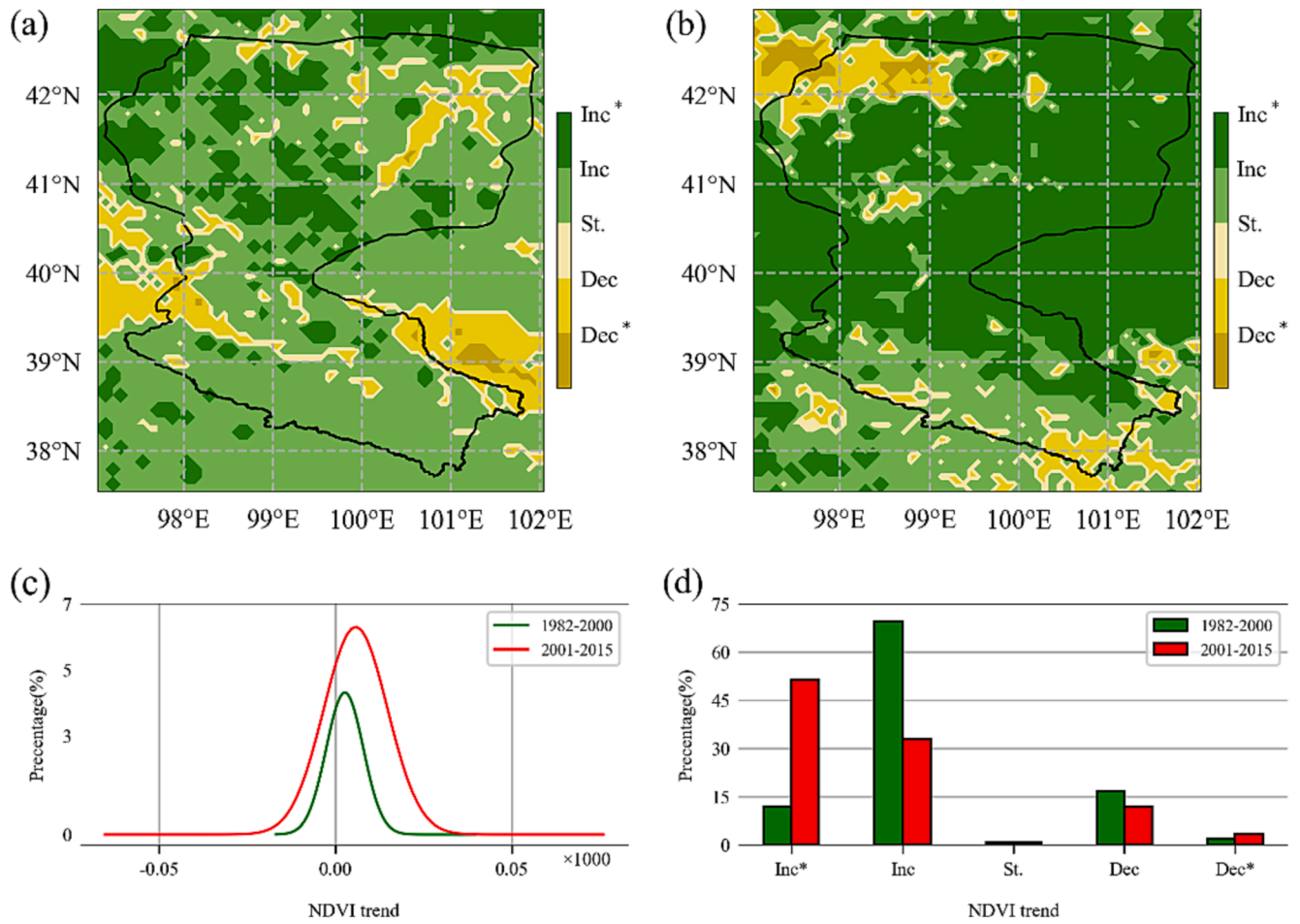

Fig. 3. Trends of NDVI in Heihe River Basin during the periods of 1982–2000 and 2001–2015. (a) The trend of 1982–2000. (b) The trend of 2001–2015. (c) NDVI trend probability density function across the two periods. (d) Bar graph depicting trend significance across two periods. Inc* (significant increases; $P < 0.05$), Inc (increases), St. (stable change) Dec (decreases), and Dec* (significant decreases).

during summer and autumn significantly surpass those in winter and spring, whereas values in spring and winter are closely aligned, the same holds true for values in summer and autumn. This indicates that there is a significant difference in local vegetation change between summer and winter half year. This phenomenon is intricately linked to the regional continental climate. In the HRB, spring witnesses a rapid temperature increase, followed by a swift drop in autumn, with precipitation primarily concentrated in the summer and autumn months (Sun et al., 2015). Upon comparison, it becomes evident that the difference among maximum NDVI values across the four seasons significantly exceeds that of the mean values. This discrepancy can be primarily attributed to the dominant presence of desert regions within the entire study area, thereby diminishing the overall average NDVI levels.

In addition, we quantified the seasonal spatial variations in vegetation (Fig. 5). During spring, there is a relatively modest overall upward trend, with most regions in the upper reaches showing a slight but statistically insignificant growth, while some areas exhibit a decline. Downstream areas, conversely, display a more pronounced growth trend. In summer, the upper and middle reaches all experience a significant increase, especially in forested and agricultural regions (Li et al., 2009). Autumn also shows a noteworthy increase, particularly in agricultural regions, though the level of significance is moderate. Winter, in contrast, reveals a notably weaker overall growth trend. When combined with Fig. 4, it becomes evident that the vegetation increase in the HRB primarily concentrates during summer and autumn, mainly within the middle and upper reaches. At the same time, the regions with a significant increase in NDVI during summer exhibit the widest distribution, underscoring that vegetation improvement in the HRB basically occurs during the growing season.

Based on the comprehensive analysis presented above, it is clear that the vegetation in the HRB demonstrates noteworthy spatiotemporal variations. Specifically, spatial and seasonal distinctions underscore the complexity of vegetation dynamics in the region's ecosystem. Hence it is imperative to approach the alterations in regional vegetation and ecosystem from a complex systems perspective. Prior research has emphasized that NDVI fluctuations are influenced by a range of factors, including temperature, precipitation, and human activities (Zhu, et al., 2020; Fang et al., 2005; Qi and Luo, 2006). These multifaceted influences emphasis the complexity interplay between the regional ecosystem and its environment. Therefore, by treating regional vegetation and ecosystem changes as integral components of a broader system and analyzing the emergence of overarching system patterns within the context of complex systems, we can attain a more profound understanding of the dynamic shifts in vegetation and environmental responses within this ecosystem.

3.2. Decomposition of NDVI in HRB from the perspective of eigen microstates

Drawing on the understanding of the fundamental spatiotemporal patterns of NDVI in the HRB, we sought to gain a comprehensive insight into the basin's dynamics by introducing eigen microstates as a quantitative analytical framework. We determined the spatial distribution and temporal evolution patterns of the initial six eigen microstates of

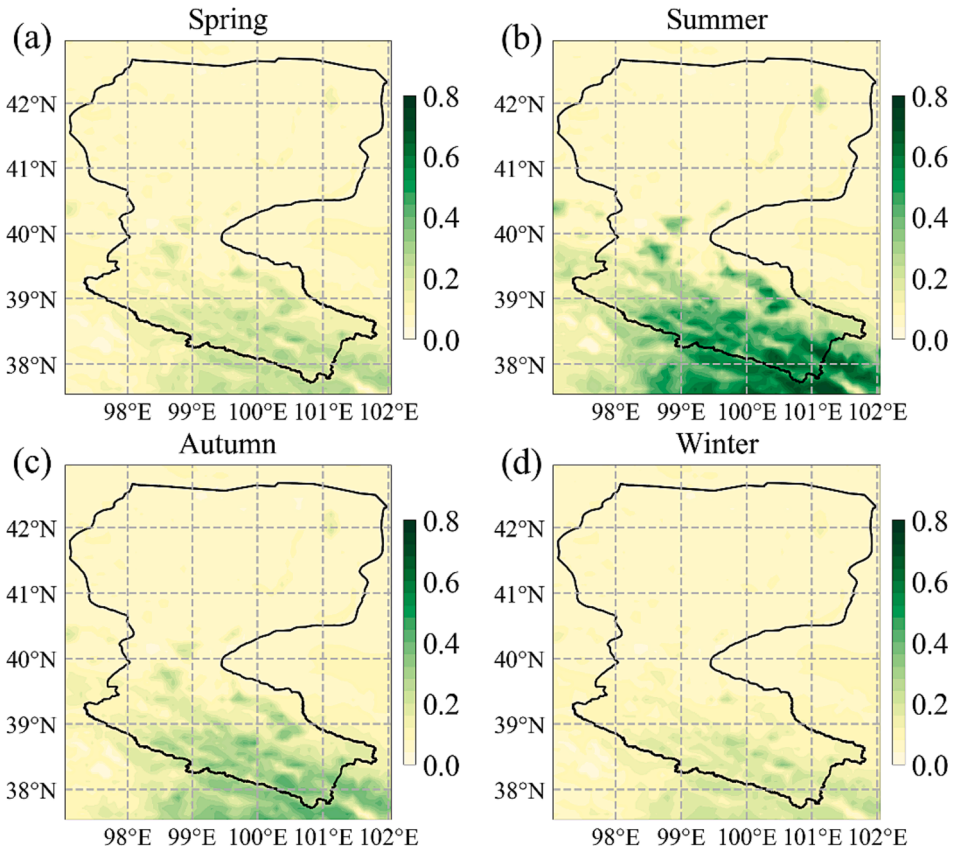

Fig. 4. Seasonal variation characteristics of NDVI in Heihe River Basin.

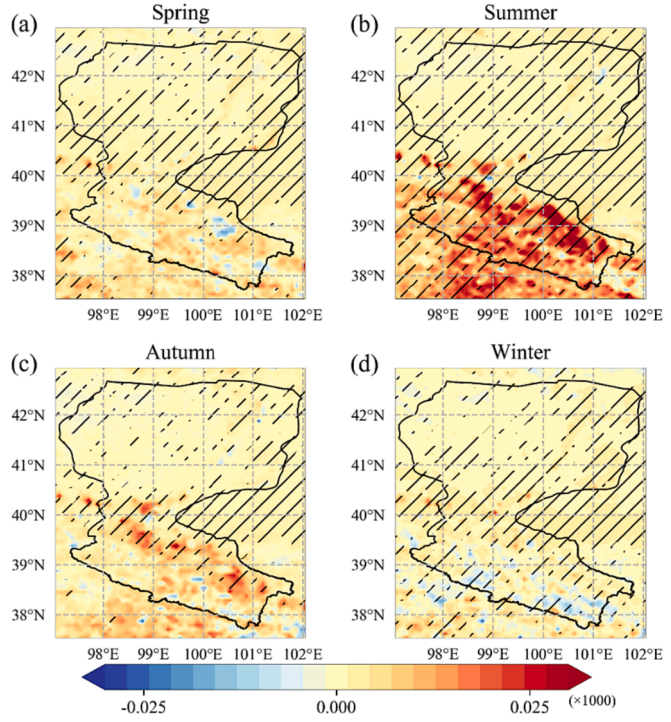

Fig. 5. Seasonal Spatial Variation Trend of NDVI in Heihe River Basin. Red signifies a positive trend, while blue signifies a negative trend, with the intensity of the color corresponding to the magnitude of the trend and the areas marked with diagonal lines indicate significance levels below 0.05. (For interpretation of the references to color in this figure legend, the reader is referred to the web version of this article.)

NDVI in the HRB (Fig. S1 and S2). In aggregate, these six microstates collectively explain 78 % of the total variance, with the first two microstates contributing significantly, accounting for 64 %. Consequently, the predominant drivers of vegetation change in this region are encapsulated within these two principal microstates. In the subsequent sections, we delve into a detailed analysis of the spatiotemporal characteristics of this first two microstates and elucidate the mechanisms underpinning their dynamics.

As depicted in Fig. 6a, EM1 demonstrates a conspicuous seasonal cyclic pattern, contributing significantly to the total variance with a proportion of 42.57 %. The spatial distribution of EM1 microstate portrays a prevailing ascending trend, albeit with sporadic irregularities in the lower HRB region. A comparison with the topographic map (Fig. 1) highlights the distinct lower elevation of this area compared to its surroundings, suggesting that these diverging trends may be linked to topographical disparities. Fig. 6c provides a visual representation of EM1′s temporal evolution. Post-2005, the evolution of EM1 reveals a perceptible upward trend. But post-2012 it demonstrates a descending pattern and the corresponding numerical values almost consistently exceed zero which elucidate a prominent indication of systemic change. Moreover, the temporal evolution in Fig. 6c captures the seasonal dynamics of vegetation growth in this region, characterized by distinct interannual patterns. Annually the results for summer closely resemble those for autumn, while those for winter align with spring. However, noticeable disparities emerge when comparing the results between spring and autumn, as well as emerge when comparing the results between winter and spring. These observations are further supported by spectral analysis findings (Fig. 7a), which unveil annual variations marked by distinct peaks and sub-peaks occurring biannually in conjunction with solar radiation fluctuations.

Fig. 6b and Fig. 6d delineate the spatial distribution and temporal evolution of EM2, the second-largest NDVI microstate in the HRB,

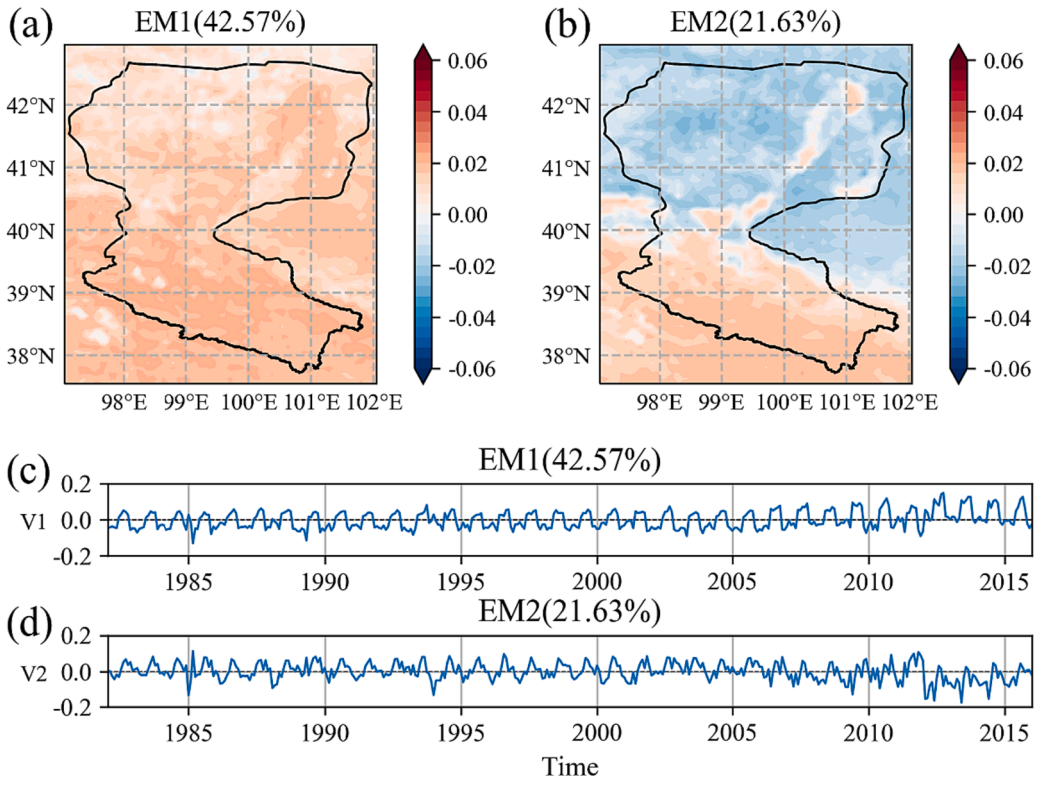

Fig. 6. Spatial distributions (a, b) and their evolutions (c, d) of the two largest eigen microstates of NDVI. EM1 and EM2 represent the first and second eigen microstate, respectively.

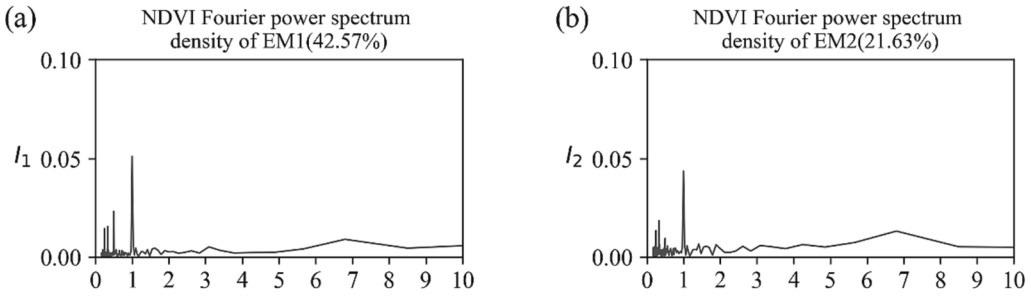

Fig. 7. Fourier power spectrum density of evolution for the two largest eigen microstates of NDVI.

contributing to 21.63 % of the variance. Similar to EM1, EM2 exhibits prominent interannual features, with the most notable cyclic pattern observed annually (Fig. 7b). Interestingly, EM2 microstate manifests obvious spatial variations, with positive values concentrated in the middle and upper reaches as well as along the primary channel of the lower reaches, while negative values prevail elsewhere. These disparities appear linked to water resources, although the combined influence of other climate variables and human activities must not be discounted (Qi and Luo, 2006; Li et al., 2013). In Fig. 6d, a distinct pattern emerges, characterized by a pronounced decline in fluctuations post-2005 and a notable increase post-2012. Remarkably, the values of the evolution during 2012–2015 consistently fall below zero, indicating a clear systemic transformation. By considering the previous insights presented in Fig. 6c, we establish that the ecosystem of the HRB experienced a continuous period of growth around 2011. This upward trajectory persisted until 2012, eventually resulting in a systemic shift, as depicted in Fig. 6c and Fig. 6d. However, a comprehensive understanding of the specific physical mechanisms underlying this phenomenon necessitates further examination using abundant data.

The aforementioned findings affirm the reliability of eigen microstates in assessing NDVI with the initial six microstates collectively explain nearly 80 % of the total variance. Concurrently, the spatial distribution analysis of EM1 corroborates a consistent NDVI increase in specified area (Fig. 6a), while the temporal evolution results of EM1 confirms the seasonally changing NDVI patterns and a pronounced growth trend post-2000 (Fig. 6c). Furthermore, the spatial distribution patterns of both EM1 and EM2 suggest a heightened correlation between the enhanced NDVI in the HRB and the complex interplay of natural factors and human activities that influence water resource availability.

3.3. Attribution analysis of NDVI changes in HRB

Climatic parameters, specifically temperature and precipitation, unequivocally stand out as the predominant factors influencing vegetation. In previous research, scholars typically employed correlation analysis or regression analysis to explore the connection between NDVI and temperature alongside precipitation within a reductionist paradigm (He et al., 2022; Ju and Masek, 2016). Our study introduced several enhancements. Firstly, we conducted a comprehensive statistical analysis encompassing the mean and standard deviation of crucial

meteorological and environmental parameters (temperature, precipitation and runoff) in the HRB (Fig. S3). The spatial distribution outcomes revealed conspicuous differences in temperature, precipitation and surface runoff between the upper the middle-to-lower regions of the HRB. Surface runoff exhibited a conspicuous rise solely in the fore mountain runoff collection area in the upper reaches, characterized by an annual average temperature below 0℃ and predominant precipitation exceeding 1.5 mm. Conversely, a divergent pattern was evident in the middle and lower reaches (Fig. S3). In the realm of interannual variability, precipitation exhibits a subtle upward trend ($k = 0.0017$, $R^2 = 0.1194$), while the ascending trajectory of temperature is more pronounced ($k = 0.0425$, $R^2 = 0.4527$) (Fig. S4).

In addition, through correlation and multivariate linear regression analyses, precipitation emerges as the most responsive element to variations in vegetation coverage within the HRB and this sensitivity can be attributed to the vertical zonation, high altitude, and low temperatures prevalent in the upper reaches of the HRB (Ma et al., 2006). As precipitation and temperature increase, vegetation growth in this region gains a distinct advantage, with the collective impact of temperature and precipitation exerting a substantial influence on the upper reaches (You et al., 2018). Notably, in the middle and lower reaches, oasis vegetation exhibits a notable spatial correlation with water system distribution and surface runoff (Xiao et al., 2015). In contrast, non-oasis vegetation experiences a more intricate interplay of temperature and precipitation effects. This complexity arises from the prevalence of farmland and protective forests in the middle reaches, primarily influenced by irrigation and water storage projects (Nian et al., 2014; Zhu et al., 2020). Downstream vegetation, concentrated along riverbanks, is directly impacted by surface runoff (Ding et al., 2017). Conclusively, for the intricately structured geography of the HRB, temperature, precipitation, and surface runoff emerge as the principal determinants significantly shaping the distribution and growth of vegetation in this region.

Despite the consistent spatial distribution of the standard deviation and mean of each variable, their alignment with the spatial distribution of NDVI eigen microstates is not substantial (EM1 and EM2) (Fig. 6ab). Especially noteworthy is the substantial post-2000 upsurge in NDVI, which evidently cannot be solely attributed to meteorological variables (Fig. S4 and Fig. 2). This finding explicates the limitations of relying merely on a single meteorological variable to explain changes in NDVI.

In fact, China initiated a series of ecological preservation initiatives in the HRB post-2000, such as ecological water transfer, strategic forest protection projects, and land conversion to forests and grasslands (Chen et al., 2014; Ding et al., 2017; Fan et al., 2018). These ecological undertakings have ameliorated the ecological milieu in the basin, leading to an augmentation in vegetation cover (Li et al., 2017; Fan et al., 2018; Chang et al., 2011). Recognizing the crucial role of water resources in nurturing vegetation in arid regions (Xiao et al., 2015; Nian et al., 2014), there has been ongoing debate regarding the choice of methodology and variables to gauge water's influence on vegetation.

In our study, we calculated the mean and standard deviation of soil moisture content across four layers, guided by the spatial distribution pattern evident in the second most prominent mode of NDVI (EM2) (Fig. S5). Our findings indicate a relatively congruent spatial alignment between soil water distribution, original NDVI values, and EM2 distribution. Subsequently, we performed a comprehensive examination of the eigen microstates within the four soil moisture layers. In terms of spatial distribution, the upper reaches exhibit a prominent positive trend in soil water content, and the second and third layers of soil moisture closely mirror the spatial distribution of irrigated farmland within the HRB. To put it simply, when considering spatial aspects, the microstate in soil moisture content across these four layers closely correspond with those observed in the NDVI (Fig. 8). We then proceeded to conduct a temporal analysis, independently fitting the outcomes of the second microstate for soil moisture within the four layers and the second microstate of NDVI separately (Fig. 9). Fig. 9 illustrates that, except for the initial soil moisture layer, the correlation between the second

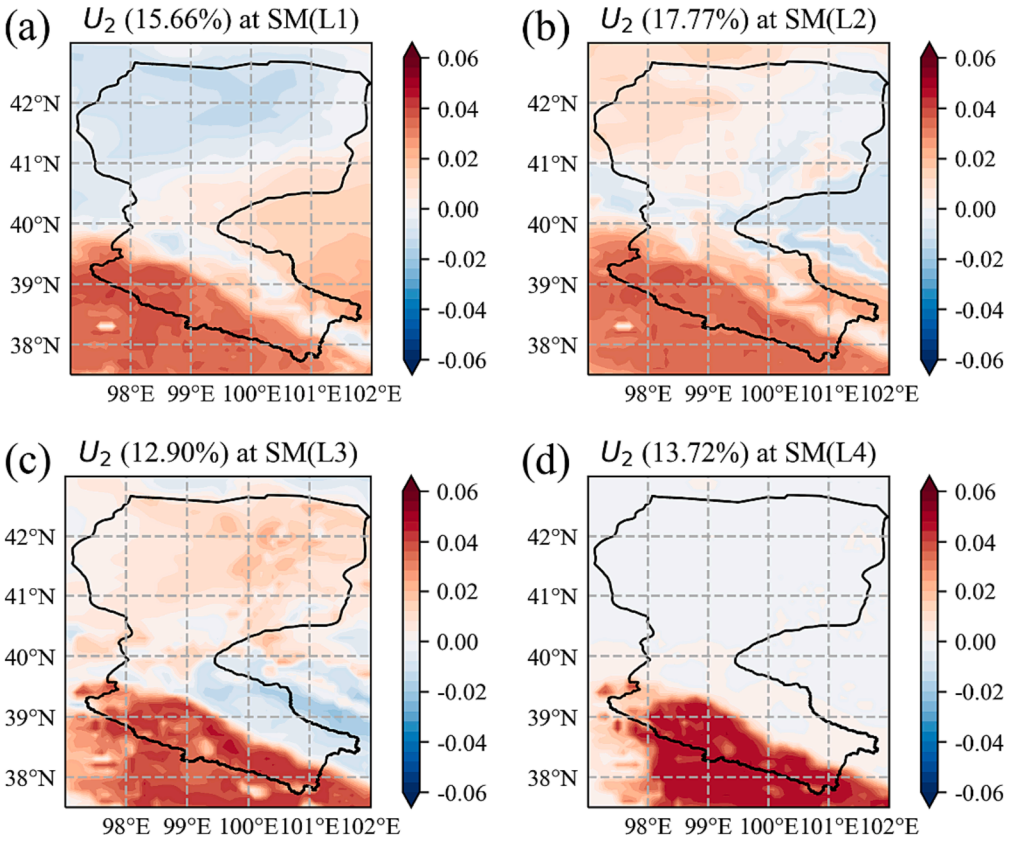

Fig. 8. Spatial distributions of eigen microstates of 4-layer-SM (a, b, c, d).

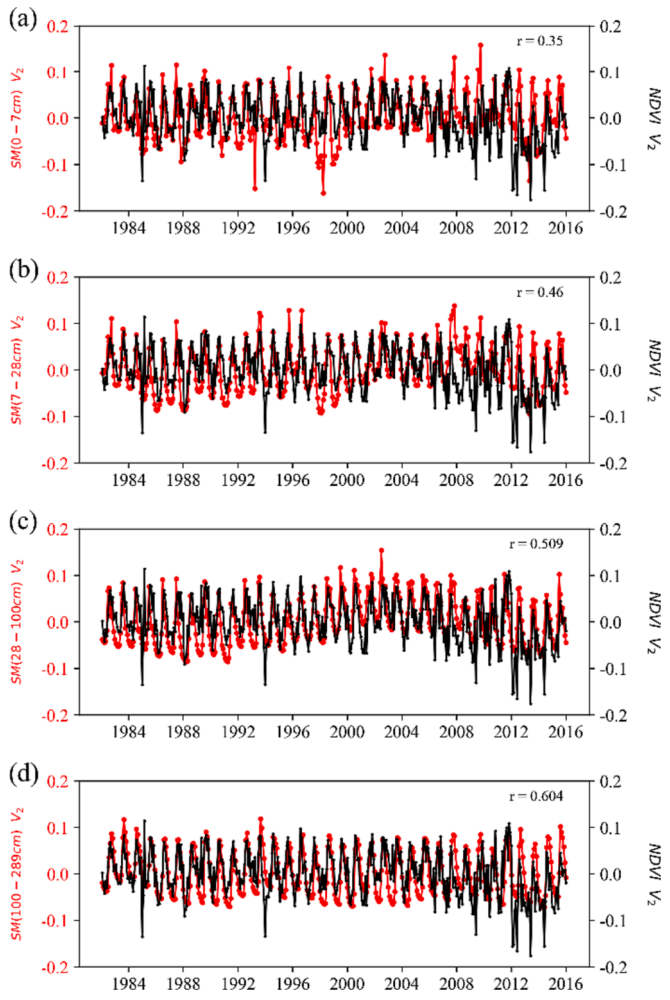

Fig. 9. Correlation comparison between the evolution V2 of 4-layer-SM (a, b, c, d) and the evolution V2 of NDVI.

microstate of NDVI and the second one of soil moisture consistently registers 0.5 or higher, with the strength of this correlation increasing as soil depth increases.

In summary, we commenced with a meticulous data analysis coupled with feature decomposition techniques, enabling us to elucidate the substantial role of soil moisture within the HRB. This contribution surpasses that of precipitation, humidity, and temperature as observed in prior research, in terms of enhancing vegetation. The underlying physical mechanism behind this phenomenon is rooted in soil moisture's ability to encapsulate the amalgamation of natural precipitation and anthropogenic influences, such as irrigation and ecological water transfers. Consequently, it plays a vital role in providing a more precise representation of water accessibility for vegetation.

4. Discussion

4.1. Soil moisture dominates vegetation growth

A recent study has also shown that soil moisture as the primary driver influencing vegetation growth in Eurasian drylands (Zhang et al., 2023). During drought events, vegetation structure parameters experience water stress attributable to elevated atmospheric water demand and constrained water supply from soil reservoirs. Not only that, soil moisture emerges as a primary determinant influencing the light-use efficiency in dryland vegetation, alongside the vegetation factor. Consequently, arid zone vegetation plays a pivotal role in steering the global trend of increased vegetation productivity (Wang et al., 2023). This global perspective aligns with the findings of our study, further substantiating the validity of our eigen microstate analysis approach. Therefore, we underscore the heightened significance of deep soil moisture in fostering vegetation growth, attributable to two key factors. Firstly, the study area's location in an arid and semi-arid region, characterized by rapid surface soil moisture evaporation. Secondly, the presence of relatively deep root absorption zones in both desert and mountain forest vegetation within the region (Li et al., 2013; Ding et al., 2017; Fan et al., 2018). Additionally, our research uncovers a time lag effect in vegetation enhancement due to soil moisture in the HRB region, with this lag period peaking at around one month (Fig. 10).

4.2. Uncertainty analysis

It should be noted that we utilize soil moisture data at a $0.1°\times0.1°$ resolution in our study. The eigen microstate method demonstrates favorable performance at this resolution and exhibits stability in analyzing HRB. Subsequently, we resampled the soil moisture to achieve a spatial resolution consistent with NDVI, set at $1/12°\times1/12°$. The results showed that the spatial distribution of soil moisture data pre- and post-resampling exhibited substantial consistency (Fig. S6 and S7). Following this, an eigen microscopic decomposition of the resampled data was executed. A comparison of spatial modes and temporal evolutions with pre-resampling results revealed no significant feature alterations. Notably, the temporal evolution exhibited an almost 100 % consistency before and after resampling (Fig. S8, Fig. S9).

However, it is important to note that the use of low-resolution data introduces the possibility of inadequate capture of intricate details and geographical complexities. Given the intricate topography of the HRB, the discernment of localized variations in vegetation cover may be insufficient, leading to distorted and obscured outcomes. And with coarser spatial resolution, surface features may be averaged, making it difficult to distinguish between different feature types. This can be problematic about the delicate relationship between soil moisture and vegetation cover. Future improvements will be considered based on specific research questions addressed in subsequent work.

5. Conclusion

This study utilizes remote sensing observation data and meteorological reanalysis data to establish a robust analytical framework for investigating ecosystem complexity and the dynamics of vegetation evolution. We apply eigen microstates and a range of analytical techniques within this framework. The developed eigen microstate method effectively decomposes NDVI microstates in conjunction with pertinent meteorological and environmental variables, elucidating their overall distribution characteristics, seasonal patterns, and interrelationships.

Upon the results of NDVI by eigen microstates, we discern that the ecosystem in the study area remains within a relatively stable phase of vegetation improvement. More importantly, the NDVI eigen microstate EM1 demonstrates consistency with both the overall vegetation improvement trend in the study area and the original data trend. Meanwhile, the NDVI eigen microstate EM2 reveals the main role of soil moisture in enhancing vegetation in arid regions. Soil moisture, being a multifaceted factor influenced by natural and human factors on water resources, displays superior explanatory power for vegetation growth in the study area when compared to individual meteorological variables. Additionally, we identify a one-month lag in the response of vegetation growth to soil moisture in the study area, with sensitivity increasing as soil moisture levels deepen. The methodologies and findings of this study hold the potential to advance the application of statistical physics within ecology and contribute to the field of ecological environment management.

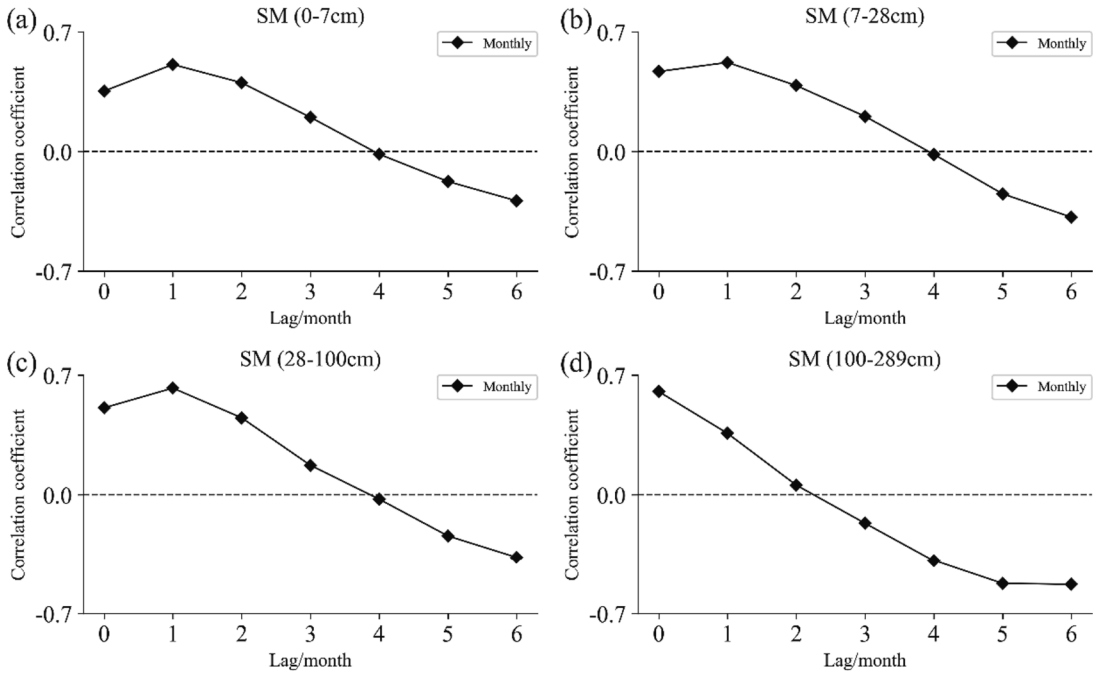

Fig. 10. The evolution V2 of NDVI exhibits a lag with respect to the evolution V2 of soil moisture.

CRediT authorship contribution statement

Xu Wang: Methodology, Writing – original draft, Writing – review & editing. **Hao Fan:** Conceptualization, Investigation, Writing – original draft, Writing – review & editing. **Xiaosong Chen:** Methodology, Software, Writing – original draft, Writing – review & editing. **Yiran Xie:** Methodology, Writing – review & editing. **Hongyu Wang:** Data curation, Methodology, Writing – review & editing.

Declaration of competing interest

The authors declare that they have no known competing financial interests or personal relationships that could have appeared to influence the work reported in this paper.

Data availability

Data will be made available on request.

Acknowledgements

This study was supported by the National Key R&D Program of China (grant 2023YFE0109000), the National Natural Science Foundation of China (grants 12135003 and 42205178).

Appendix A. Supplementary data

Supplementary data to this article can be found online at https://doi.org/10.1016/j.ecolind.2024.111689.

References

Chang, Y.S., Bao, D., Bao, Y.H., 2011. Satellite monitoring of the ecological environment recovery effect in the heihe river downstream region for the last 11years. Procedia Environ. Sci. 10, 2385–2392. https://doi.org/10.1016/j.proenv.2011.09.371.

Chen, X.H., Duan, Z.H., Luo, T.F., 2014. Changes in soil quality in the critical area of desertification surrounding the Ejina O. Environ. Earth. Sci. 72 (7), 2643–2654. https://doi.org/10.1007/s12665-014-3171-3.

Chen, X.J., Ying, N., Chen, D., Zhang, Y.W., Lu, B., Fan, J.F., Chen, X.S., 2021. Eigen microstates and their evolution of global ozone at different geopotential heights. Chaos 31 (7), 071102. https://doi.org/10.1063/5.0058599.

Cheng, G.D., Li, X., Zhao, W.Z., Xu, Z.M., Feng, Q., Xiao, S.C., Xiao, H.L., 2014. Integrated study of the water-ecosystem-economy in the Heihe River Basin. Natl. Sci. Rev. 1 (3), 413–428. https://doi.org/10.1093/nsr/nwu017.

Chu, H.S., Venevsky, S., Wu, C., Wang, M.H., 2019. NDVI-based vegetation dynamics and its response to climate changes at Amur-Heilongjiang River Basin from 1982 to 2015. Sci. Total Environ. 650, 2051–2062. https://doi.org/10.1016/j.scitotenv.2018.09.115.

Ciais, P., Reichstein, M., Viovy, N., Granier, A., Ogée, J., Allard, V., Aubinet, M., Buchmann, N., Bernhofer, C., Carrara, A., Chevallier, F., De Noblet, N., Friend, A.D., Friedlingstein, P., Grünwald, T., Heinesch, B., Keronen, P., Knohl, A., Krinner, G., Loustau, D., Manca, G., Matteucci, G., Miglietta, F., Ourcival, J.M., Papale, D., Pilegaard, K., Rambal, S., Seufert, G., Soussana, J.F., Sanz, M.J., Schulze, E.D., Vesala, T., Valentini, R., 2005. Europe-wide reduction in primary productivity caused by the heat and drought in 2003. Nature 437 (7058), 529–533. https://doi.org/10.1038/nature03972.

De Jong, R., Schaepman, M.E., Furrer, R., De Bruin, S., Verburg, P.H., 2013. Spatial relationship between climatologies and changes in global vegetation activity. Global Change Biol. 19 (6), 1953–1964. https://doi.org/10.1111/gcb.12193.

Ding, J.Y., Zhao, W.W., Daryanto, S., Wang, L.X., Fan, H., Feng, Q., Wang, Y.P., 2017. The spatial distribution and temporal variation of desert riparian forests and their influencing factors in the downstream Heihe River basin, China. Hydrol. Earth Syst. Sc. 21 (5), 2405–2419. https://doi.org/10.5194/hess-21-2405-2017.

Fan, H., Zhao, W.W., Daryanto, S., Fu, B.J., Wang, S., Wang, Y.P., 2018. Vertical distributions of soil organic carbon and its influencing factors under different land use types in the desert riparian zone of downstream Heihe River Basin, China. J. Geophys. Res. Atmos. 123 (14), 7741–7753. https://doi.org/10.1029/2018JD028268.

Fan, H., Wang, Y., Zhao, C.F., Yang, Y.K., Yang, X.C., Sun, Y., Jiang, S.Y., 2021. The role of primary emission and transboundary transport in the air quality changes during and after the COVID-19 lockdown in China. Geophys. Res. Lett. 48 (7), e2020GL091065 https://doi.org/10.1029/2020GL091065.

Fan, H., Yang, X.C., Zhao, C.F., Yang, Y.K., Shen, Z.Y., 2023. Spatiotemporal variation characteristics of global fires and their emissions. Atmos. Chem. Phys. 23 (13), 7781–7798. https://doi.org/10.5194/acp-23-7781-2023.

Fang, J.Y., Piao, S.L., Zhou, L.M., He, J.S., Wei, F.Y., Myneni, R.B., Tucker, C.J., Tan, K., 2005. Precipitation patterns alter growth of temperate vegetation. Geophys. Res. Lett. 32 (21), L21411. https://doi.org/10.1029/2005GL024231.

Geng, L.Y., Ma, M.G., Wang, X.F., Yu, W.P., Jia, S.Z., Wang, H.B., 2014. Comparison of eight techniques for reconstructing multi-satellite sensor time-series NDVI data sets in the Heihe River Basin, China. Remote Sens. 6, 2024–2049. https://doi.org/10.3390/rs6032024.

Guo, J.P., Zhang, J., Yang, K., Liao, H., Zhang, S.D., Huang, K.M., Lv, Y.M., Shao, J., Yu, T., Tong, B., Li, J., Su, T.N., Yim, S.H.L., Stoffelen, A., Zhai, P.M., Xu, X.F., 2021. Investigation of near-global daytime boundary layer height using high-resolution radiosondes: first results and comparison with ERA5, MERRA-2, JRA-55, and NCEP-2 reanalyses. Atmos. Chem. Phys. 21 (22), 17079–17097. https://doi.org/10.5194/acp-21-17079-2021.

He, B., Wu, X., Liu, K., Yao, Y.Z., Chen, W.J., Zhao, W., 2022. Trends in forest greening and its spatial correlation with bioclimatic and environmental factors in the Greater Mekong Subregion from 2001 to 2020. Remote Sens. 14 (23), 5982. https://doi.org/10.3390/rs14235982.

Ichii, K., Kawabata, A., Yamaguchi, Y., 2002. Global correlation analysis for NDVI and climatic variables and NDVI trends: 1982–1990. Int. J. Remote Sens. 23 (18), 3873–3878. https://doi.org/10.1080/01431160110119416.
Ives, A.R., Carpenter, S.R., 2007. Stability and diversity of ecosystems. Science 317 (5834), 58–62. https://doi.org/10.1126/science.1133258.
Jiang, P., Ding, W.G., Yuan, Y., Ye, W.F., Mu, Y.J., 2022. Interannual variability of vegetation sensitivity to climate in China. J. Environ. Manage. 301, 113768 https://doi.org/10.1016/j.jenvman.2021.113768.
Jiang, L.L., Jiapaer, G., Bao, A.M., Guo, H., Ndayisaba, F., 2017. Vegetation dynamics and responses to climate change and human activities in Central Asia. Sci. Total Environ. 599, 967–980. https://doi.org/10.1016/j.scitotenv.2017.05.012.
Jiang, X.H., Liu, C.M., 2010. The influence of water regulation on vegetation in the lower Heihe River. J. Geogr. Sci. 20 (5), 701–711. https://doi.org/10.1007/s11442-010-0805-6.
Jiang, W.G., Yuan, L.H., Wang, W.J., Cao, R., Zhang, Y.F., Shen, W.M., 2015. Spatio-temporal analysis of vegetation variation in the Yellow River Basin. Ecol. Indic. 51, 117–126. https://doi.org/10.1016/j.ecolind.2014.07.031.
John, R., Chen, J.Q., Kim, Y., Ou-yang, Z.T., Xiao, J.F., Park, H., Shao, C.L., Zhang, Y.Q., Amarjargal, A., Batkhshig, O., Qi, J.G., 2016. Differentiating anthropogenic modification and precipitation-driven change on vegetation productivity on the Mongolian Plateau. Landscape Ecol. 31 (3), 547–566. https://doi.org/10.1007/s10980-015-0261-x.
Ju, J.C., Masek, J.G., 2016. The vegetation greenness trend in Canada and US Alaska from 1984–2012 Landsat data. Remote Sens. Environ. 176, 1–16. https://doi.org/10.1016/j.rse.2016.01.001.
Kariyeva, J., van Leeuwen, W.J.D., 2011. Environmental drivers of NDVI-based vegetation phenology in Central Asia. Remote Sens. 3 (2), 203–246. https://doi.org/10.3390/rs3020203.
Lamchin, M., Lee, W.K., Jeon, S.W., Wang, S.W., Lim, C.H., Song, C., Sung, M.J., 2018. Long-term trend and correlation between vegetation greenness and climate variables in Asia based on satellite data. Sci. Total Environ. 618, 1089–1095. https://doi.org/10.1016/j.scitotenv.2017. 09.145.
Lenton, T.M., Rockström, J., Gaffney, O., Rahmstorf, S., Richardson, K., Steffen, W., Schellnhuber, H.J., 2019. Climate tipping points-too risky to bet against. Nature 575 (7784), 592–595. https://doi.org/10.1038/d41586-019-03595-0.
Li, Y.R., Cao, Z., Long, H.L., Liu, Y.S., Li, W.J., 2017. Dynamic analysis of ecological environment combined with land cover and NDVI changes and implications for sustainable urban–rural development: the case of Mu Us Sandy Land, China. J. Clean. Prod. 142, 697–715. https://doi.org/10.1016/j.jclepro.2016.09.011.
Li, X., Cheng, G.D., Liu, S.M., Xiao, Q., Ma, M.G., Jin, R., Che, T., Liu, Q.H., Wang, W.Z., Qi, Y., Wen, J.G., Li, H.Y., Zhu, G.F., Guo, J.W., Ran, Y.H., Wang, S.G., Zhu, Z.L., Zhou, J., Hu, X.L., Xu, Z.W., 2013. Heihe watershed allied telemetry experimental research (HiWATER): scientific objectives and experimental design. B. Am. Meteorol. Soc. 94 (8), 1145–1160. https://doi.org/10.1175/BAMS-D-12-00154.1.
Li, X., Li, X.W., Li, Z.Y., Ma, M.G., Wang, J., Xiao, Q., Liu, Q., Che, T., Chen, E., Yan, G.J., Hu, Z.Y., Zhang, L.X., Chu, R.Z., Su, P.X., Liu, Q.H., Liu, S.M., Wang, J.D., Niu, Z., Chen, Y., Jin, R., Wang, W.Z., Ran, Y.H., Xin, X.Z., Ren, H.Z., 2009. Watershed allied telemetry experimental research. J. Geophys. Res. Atmos. 114, D22103. https://doi.org/10.1029/2008JD 011590.
Li, M.X., Wu, P.L., Ma, Z.G., 2020. A comprehensive evaluation of soil moisture and soil temperature from third-generation atmospheric and land reanalysis data sets. Int. J. Climatol. 40 (13), 5744–5766. https://doi.org/10.1002/joc.6549.
Liu, T., Chen, D., Yang, L., Meng, J., Wang, Z.C.L., Ludescher, J., Fan, J.F., Yang, S.N., Chen, D.L., Kurths, J., Chen, X.S., Havlin, S., Schellnhuber, H.J., 2023. Teleconnections among tipping elements in the Earth system. Nat. Clim. Change 13 (1), 67–74. https://doi.org/10.1038/s41558-022-01558-4.
Liu, Y.L., Lei, H.M., 2015. Responses of natural vegetation dynamics to climate drivers in China from 1982 to 2011. Remote Sens. 7 (8), 10243–10268. https://doi.org/10.3390/rs70810243.
Ma, M.G., Frank, V., 2006. Interannual variability of vegetation cover in the Chinese Heihe River Basin and its relation to meteorological parameters. Int. J. Remote Sens. 27 (16), 3473–3486. https://doi.org/10.1080/01431160600593031.
Nian, Y.Y., Li, X., Zhou, J., Hu, X.L., 2014. Impact of land use change on water resource allocation in the middle reaches of the Heihe River Basin in northwestern China. J. Arid Land 6 (3), 273–286. https://doi.org/10.1007/s40333-013-0209-4.
Park, H.S., Sohn, B.J., 2010. Recent trends in changes of vegetation over East Asia coupled with temperature and rainfall variations. J. Geophys. Res. Atmos. 115, D14101. https://doi.org/10.1029/2009JD012752.
Peng, S.S., Chen, A.P., Xu, L., Cao, C.X., Fang, J.Y., Myneni, R.B., Pinzon, J.E., Tucker, C. J., Piao, S.L., 2011. Recent change of vegetation growth trend in China. Environ. Res. Lett. 6 (4), 044027 https://doi.org/10.1088/1748-9326/6/4/044027.
Peñuelas, J., Filella, I., Comas, P., 2002. Changed plant and animal life cycles from 1952 to 2000 in the Mediterranean region. Glob. Change Biol. 8 (6), 531–544. https://doi.org/10.1046/j.1365-2486.2002.00489.x.
Peylin, P., Bousquet, P., Le Quéré, C., Sitch, S., Friedlingstein, P., McKinley, G., Gruber, N., Rayner, P., Ciais, P., 2005. Multiple constraints on regional CO2 flux variations over land and oceans. Global Biogeochem. Cy. 19, GB1011. https://doi.org/10.1029/2003GB002214.
Piao, S.L., Wang, X.H., Ciais, P., Zhu, B., Wang, T., Liu, J., 2011. Changes in satellite-derived vegetation growth trend in temperate and boreal Eurasia from 1982 to 2006. Glob. Change Biol. 17 (10), 3228–3239. https://doi.org/10.1111/j.1365-2486.2011.02419.x.
Qi, S.Z., Luo, F., 2006. Land-use change and its environmental impact in the Heihe River Basin, arid northwestern China. Environ. Geol. 50 (4), 535–540. https://doi.org/10.1007/s00254-006-0230-4.
Rohrer, M., Martius, O., Raible, C.C., Brönnimann, S., 2020. Sensitivity of blocks and cyclones in ERA5 to spatial resolution and definition. Geophys. Res. Lett. 47 (7), e2019GL085582 https://doi.org/10.1029/2019GL085582.
Sun, Y., Hu, G.K., Zhang, Y.W., Lu, B., Lu, Z.H., Fan, J.F., Li, X.T., Deng, Q.M., Chen, X.S., 2021. Eigen microstates and their evolutions in complex systems. Commun. Theor. Phys. 73 (6), 065603 https://doi.org/10.1088/1572-9494/abf127.
Sun, W.C., Song, H., Yao, X.L., Ishidaira, H., Xu, Z.X., 2015. Changes in remotely sensed vegetation growth trend in the Heihe Basin of arid northwestern China. PLoS One 10 (8), e0135376.
Verbesselt, J., Hyndman, R., Newnham, G., Culvenor, D., 2010. Detecting trend and seasonal changes in satellite image time series. Remote Sens. Environ. 114 (1), 106–115. https://doi.org/10.1016/j.rse.2009.08.014.
Virtanen, R., Luoto, M., Rämä, T., Mikkola, K., Hjort, J., Grytnes, J.A., Birks, H.J.B., 2010. Recent vegetation changes at the high-latitude tree line ecotone are controlled by geomorphological disturbance, productivity and diversity. Global Ecol. Biogeogr. 19 (6), 810–821. https://doi.org/10.1111/j.1466-8238.2010.00570.x.
Wang, S., Fu, B.J., Wei, F.L., Piao, S.L., Maestre, F.T., Wang, L.X., Jiao, W.Z., Liu, Y.X., Li, Y., Li, C.J., Zhao, W.W., 2023. Drylands contribute disproportionately to observed global productivity increases. Sci. Bull. 68 (2), 224–232. https://doi.org/10.1016/j.scib.2023.01.014.
Wu, Z.Y., Feng, H.H., He, H., Zhou, J.H., Zhang, Y.L., 2020. Evaluation of soil moisture climatology and anomaly components derived from ERA5-Land and GLDAS-2.1 in China. Water. Resour. Manag. 35, 629–643. https://doi.org/10.1007/s11269-020-02743-w.
Xiao, S.C., Xiao, H.L., Peng, X.M., Song, X., 2015. Hydroclimate-driven changes in the landscape structure of the terminal lakes and wetlands of the China's Heihe River Basin. Environ. Monit. Assess. 187 (1), 4091. https://doi.org/10.1007/s10661-014-4091-0.
Xu, H.J., Wang, X.P., Yang, T.B., 2017. Trend shifts in satellite-derived vegetation growth in Central Eurasia, 1982–2013. Sci. Total Environ. 579, 1658–1674. https://doi.org/10.1016/j.scitotenv. 2016.11.182.
Xu, G., Zhang, H.F., Chen, B.Z., Zhang, H.R., Innes, J.L., Wang, G.Y., Yan, J.W., Zheng, Y. H., Zhu, Z.C., Myneni, R.B., 2014. Changes in vegetation growth dynamics and relations with climate over China's landmass from 1982 to 2011. Remote Sens. 6 (4), 3263–3283. https://doi.org/10.3390/rs6043263.
You, N., Meng, J.J., Zhu, L.K., 2018. Sensitivity and resilience of ecosystems to climate variability in the semi-arid to hyper-arid areas of Northern China: a case study in the Heihe River Basin. Ecol. Res. 33 (1), 161–174. https://doi.org/10.1007/s11284-017-1543-3.
You, N.S., Meng, J.J., Zhu, L.J., Jiang, S., Zhu, L.K., Li, F., Kuo, L.J., 2020. Isolating the impacts of land use/cover change and climate change on the GPP in the Heihe River Basin of China. J. Geophys. Res. Biogeo. 125 (10), e2020JG005734 https://doi.org/10.1029/2020JG005734.
Yuan, L.H., Chen, X.Q., Wang, X.Y., Xiong, Z., Song, C.Q., 2019a. Spatial associations between NDVI and environmental factors in the Heihe River Basin. J. Geogr. Sci. 29 (9), 1548–1564. https://doi.org/10.1007/s10661-014-4091-0.
Yuan, W.P., Zheng, Y., Piao, S.L., Ciais, P., Lombardozzi, D., Wang, Y.P., Ryu, Y., Chen, G.X., Dong, W.J., Hu, Z.M., Jain, A.K., Jiang, C.Y., Kato, E., Li, S.H., Lienert, S., Liu, S.G., Nabel, J.E.M.S., Qin, Z.C., Quine, T., Sitch, S., Smith, W.K., Wang, F., Wu, C.Y., Xiao, Z.Q., Yang, S., 2019b. Increased atmospheric vapor pressure deficit reduces global vegetation growth. Sci. Adv. 5 (8), eaax1396 https://doi.org/10.1126/sciadv.aax1396.
Zang, C.F., Liu, J.G., 2013. Trend analysis for the flows of green and blue water in the Heihe River basin, northwestern China. J. Hydrol. 502, 27–36. https://doi.org/10.1016/j.jhydrol.2013.08.022.
Zhang, Y.W., Fan, J.F., Li, X.T., Liu, W.Q., Chen, X.S., 2020. Evolution mechanism of principal modes in climate dynamics. New J. Phys. 22 (9), 093077 https://doi.org/10.1088/1367-2630/abb89a.
Zhang, Y., Zhang, Y.J., Lian, X., Zheng, Z.T., Zhao, G., Zhang, T., Xu, M.J., Huang, K., Chen, N., Li, J., Piao, S.L., 2023. Enhanced dominance of soil moisture stress on vegetation growth in Eurasian drylands. Natl. Sci. Rev. 10 (8), nwad108 https://doi.org/10.1093/nsr/nwad108.
Zhao, L., Dai, A.G., Dong, B., 2018. Changes in global vegetation activity and its driving factors during 1982–2013. Agr. Forest Meteorol. 249, 198–209. https://doi.org/10.1016/j.agrformet. 2017.11. 013.
Zhu, L.J., Meng, J.J., Zhu, L.K., 2020. Applying Geodetector to disentangle the contributions of natural and anthropogenic factors to NDVI variations in the middle reaches of the Heihe River Basin. Ecol. Indic. 117, 106545 https://doi.org/10.1016/j.ecolind.2020.106545.
Zhu, Y.K., Zhang, J.T., Zhang, Y.Q., Qin, S.G., Shao, Y.Y., Gao, Y., 2019. Responses of vegetation to climatic variations in the desert region of northern China. Catena 175, 27–36. https://doi.org/10.1016/j.catena.2018.12.007.